Converging chondrogenic aggregates and melt electrowriting for the fabrication of patient-specific implants

Alessandra Di Lorenzo

1786954

Supervisor:

Assistant prof. Dr. Mylene de Ruijter

Examiner:

Prof. Dr. Jos Malda

Second examiner:

Assistant prof. Dr. Jaqueline Lourdes Rios

Master of Science in Regenerative Medicine and Technology

September 2023

Abstract

Articular cartilage defects are common and they strongly affect the quality of life of the patients and lead to a significan healthcare burden. Current treatments are hampered by the avascularity of the tissue and eventually do not provide an appropriate tissue repair, especially in the long term. Biofabrication techniques have been taking hold in the cartilage regeneration field to develop potential alternatives to current treatments. However, scaffolds lack to resemble the native tissue both biologically and in terms of mechanical properties. The inclusion of cells in scaffolds was shown to allow degradation to occur in tandem with tissue formation and the use of 3D culture systems can potentially lead to a more precise resemblance of the natural cell microenvironment. The aim of this study was to use extrusion-based bioprinting to deposit Articular cartilage chondroprogenitor cells (ACPCs) aggregates included in gelatin methacryloyl (gelMA) inside melt electrowritten “box-like” scaffolds. We aimed to reproduce both the cartilage component and the fibre-reinforcing component of the native tissue by converging the two biofabrication techniques, together with the use for the first time of ACPCs aggregates. In this study, we bioprinted on top of flat and tilted surfaces, showing the possibility to fabricate scaffolds with anatomically relevant angles, thus shapes. The metabolic activity was investigated and no significant difference was found over 7 days, suggesting its mantainance over the evaluated period of time. Upon quantification of the aggregate viability, no significant difference was found over the same period on top of flat and tilted substrates. This study suggests that the combination of extrusion-based bioprinting of aggregates and melt electrowriting is promising to achieve implants tailored according to anatomically relevant shapes.

Layman’s summary

Injuries to the articular cartilage are common and they reduce the well-being of patients as well as having a very strong impact on the cost of medical care. As the cartilage tissue does not have any blood vessel, it is difficult to recover from the injuries with the current treatments, especially in the long term. To potentially allow the healing of the cartilage tissue, implants can be designed in the lab and they need to mimic the native tissue. Combining cells with specific materials that can come into contact with the body it may be possible to boost the repair of the tissue. In particular, the inclusion of cells can possibly allow the implants to degrade at the same time as the tissue heals. The cells can clump together to make aggregates and as a result they may produce substances in a way that resembles the native tissue better. This study aimed to make an implant for injured cartilage tissue by using two techniques. The first one is called melt electrowriting and is used to deposit materials with high resolution and with a controlled design. The second one is a technique that allows to print peculiar materials, called hydrogels, in which cell aggregates can be included. The approach consists in making aggregates by using special cells, called Articular cartilage chondroprogenitor cells (ACPCs) that can possibly become chondrocytes, include them in the hydrogel and deposit them inside the melt electrowritten implant. As real cartilage damages are not only flat, in this study we used the techniques to print on top of flat and tilted substrates, to mimic angles that better resemble real damages. After the process, we checked if the aggregates were able to survive and how well they possibly survived, over a period of 7 days. We found out that the viability and the cell metabolism was maintained constant. The results of this study suggest that the combination of these techniques is promising to allow the fabrication of implants to heal the cartilage, resemble anatomically relevant shapes.

Contents

1. Introduction

1.1 Articular cartilage structure

Articular cartilage (AC) is an avascular, aneural and alymphatic connective tissue located at the end of the bones of diarthrodial joints [1]. It has the purpose of transfering the load, providing extremely low friction between the sliding bones [1]. The tissue is mainly composed by water, collagen (90%-95% type II) and proteoglycans and the chondrocyte is the main resident cell type [2]. The function of AC is guaranteed by its peculiar collagen network structure, commonly known as "Benninghoff arcade" (Figure 1). The tangential zone provides the gliding surface for joints and the collagen fibres in the this zone are aligned parallel to the articular surface (AC). The middle zone represents the first line of resistance to the compressive forces by presenting an obliquely organized collagen structure [2]. The deep zone is pivotal to provide resistance to compressive forces as the thicker collagen fibres are aligned perpendicular to the articular surface [2].

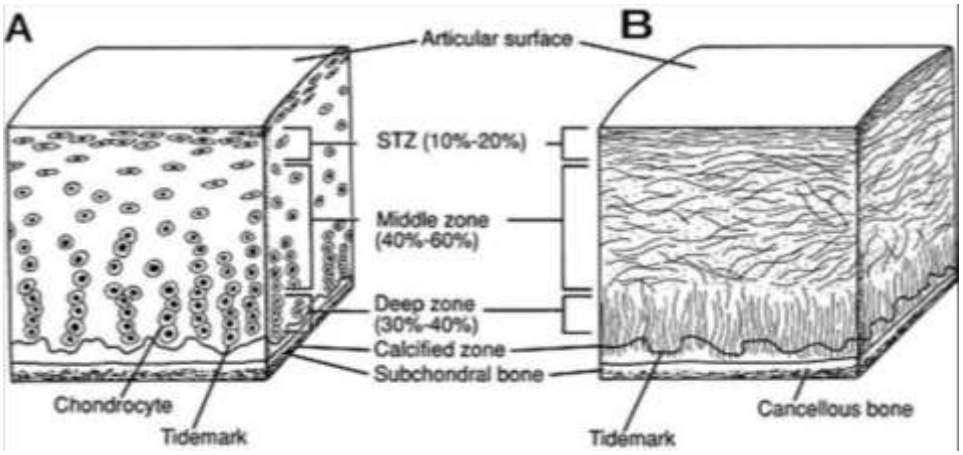

Figure 1: Schematic, cross-sectional diagram of healthy articular cartilage: A, cellular organization in the zones of articular cartilage; B, collagen fiber architecture [3].

1.2 Articular cartilage defects

Articular cartilage defects are common as they are detected in 60% to 66% of knees undergoing arthroscopy [4]. Precise determination of the incidence of AC defects is challenging as symptoms (eg. pain) versus tissue damage does not directly correlate [5].

The aethiology of AC defects is multifactorial (Table 1) and this clinical condition induces changes in the biomechanical properties and structure of the tissue, which subsequently impair the function of the joint [6]. The symptoms include pain and reduced mobility, which diminish patient's life quality [7], and significantly increases the risk of developing osteoarthritis (OA) prematurely [7]. In addition, AC regeneration is limited and contributed to the avascularity of the tissue and the high concentration of protease and cytokine inhibitors [8].

Table 1: Aetiology of AC defects of the knee [9].

Trauma (blunt impacts, traumatic patellar dislocation, polytraumatic injuries)
Axial malalignment of the knee
Partial or total meniscectomy
Instability (ACL, PCL, etc.)
Osteochondritis dissecans
Osteoarthritis
Rheumatoid arthritis
Genetic factors
Obesity
Cartilage tumours
Microtrauma

The effects of AC injuries not only affect the quality of life of the patient, but they also have a significant healthcare burden. The consequences of AC injuries include both direct and indirect cost: the direct economic impact of OA in the Netherlands in 2017, it extimated €1.2 billion, while the indirect costs related to OA accounted for 83% of the total economic burden of OA [10].

1.3 Articular cartilage regeneration strategies

During the last decades, more and more treatment approaches have been shown to improve neo-tissue formation [11]. Several classifications have been developed in order to evaluate the best approaches for AC regeneration. One of the most common methods used in The Netherlands to macroscopically

evaluate cartilage repair approaches is the International Cartilage Repair Society (ICRS) Visual Histological Assessment Scale (Table 2).

Current techniques to intervene on chondral defects include three main areas: conservative treatments, marrow stimulation treatment such as microfractures, and allograft/autograft transplantation [12]. However, these approaches aim to reduce the clinical symptoms without addressing the underlying causes, eventually not providing an appropriate tissue repair, especially in the long term.

Table 2: ICRS macroscopic evaluation of cartilage repair [13].

Cartilage repair assessment ICRS	Points
Degree of defect repair	
In level with surrounding cartilage	4
75% repair of defect depth	3
50% repair of defect depth	2
25% repair of defect depth	1
0% repair of defect depth	0
Integration to border zone	
Complete integration with surrounding cartilage	4
Demarcating border < 1 mm	3
3/4th of graft integrated, 1/4th with a notable border > 1 mm width	2
1/2 of graft integrated with surrounding cartilage, 1/2 with a notable border > 1 mm	1
From no contact to 1/4th of graft integrated with surrounding cartilage	0
Macroscopic appearance	
Intact smooth surface	4
Fibrillated surface	3
Small, scattered fissures or cracs	2
Several, small or few but large fissures	1
Total degeneration of grafted area	0
Overall repair assessment	
Grade I: normal	12
Grade II: nearly normal	11–8
Grade III: abnormal	7–4
Grade IV: severely abnormal	3–1

1.4 Biofabrication approach to articular cartilage regeneration

Biofabrication techniques are commonly used to study cartilage tissue regeneration. Biofabrication is a rapidly evolving field that combines living cells, bioactive molecules and biomaterials to fabricate biologically functional products [14]. Biofabrication allows to manufacture scaffolds with geometries tailored according to the patient-specific needs. The personalized morphology of the scaffolds has the advantage of being fabricated according to the defect. As a result, they can be optimized in terms of mechanbiology and no further cartilage resection is necessary in the process of surgical implantation [15]. Studies have investigated the incorporation of cells together with extrusion-based bioprinted soft hydrogels to achieve 3D cartilage-like matrix deposition [16]. Nevertheless, scaffolds developed in *in vitro* studies have not been able to mimic the complexity nor to fully restore the functionality of native articular cartilage [17].

In this context, the melt electrowriting (MEW) technique seems to be promising in the fabrication of cartilage implants when combinated with hydrogels. This technique allows to achieve high fibre resolution prints, which facilitate complex morphologies and thus potentially reach greater biomimicry [18].

As the mechanical properties of native AC tissue depend on both the fibrous and non-fibrous components of the extracellular matrix (ECM), the control over the fibre architecture, improves the compressive properties of the hydrogel itself and leaves space for cartilage-like matrix production [19, 20]. The presence of MEW fibres in the construct consequently provides the reinforcement of the hydrogel constructs in terms of both shear [21] and compression [19, 22].

The bio-compatible, biodegradable and injectable gelMA is a good candidate for AC regeneration [23] due to its biocompatibility and biodegradability. Furthermore, its viscosity and mechanical properties can be tuned according to the degree of substitution [39].

The choice of polycaprolactone (PCL) as a polymer for MEW printing relies on its low melting temperature and rapid solidification [37]. The mechanical properties of PCL, combined with its high biocompatibility, reproducibility and its degradation time, allow to maintain its architectural integrity and mechanical properties while cells are synthesizing new ECM [24]. The extensive use of PCL in the field of MEW printing, together with the advantages of 3D printing of bioinks allows to fabricate implants compatible biologically and in terms of stiffness for cartilage application [19].

1.5 Cell source

In biofabrication approaches to cartilage regeneration, the inclusion of cells in scaffolds was shown to allow degradation to occur in tandem with tissue formation [25]. Several cell sources have been investigated to proper mimic the native cartilage ECM as one of the major challenges is to populate the scaffold with an abundant number of cells. In this context, ACPCs are promising because of several factors such as their expansion potential and their in vitro self-renewal [26]. They have a paramount role in cartilage development, maturation and repair upon injury [26]. In addition, they show low or no expression of RUNX2, the master transcription factor for chondrocyte terminal differentiation and subsequent formation of calcified tissue [27].

The implementation of 3D culture systems overcomes the limitations of 2D cell cultures, such as limited interactions among cells, reduced responsiveness and interference with phenotype and function of the cells, leading to a more precisely resembling of the natural cell microenvironment [38].

Furthermore, the production of ECM by 3D aggregate cultures can be guided by imposing boundary conditions. A study showed that the deposition of MSCs aggregates in PCL square boxes, guided the

production of collagen network which mirrored aspects of the Benninghoff arcade structure seen in normal AC [28]. On the contrary, in unguided conditions, there was limited spatial organisation [28].

1.6 Aim

Current scaffolds fabricated to implement AC regeneration lack to mimic the mechanical properties together with not resembling the ECM architecture of the native tissue. Consequently, the initial hypothesis is that the convergence of melt electrowriting and extrusion-based bioprinting is an appropriate approach for the fabrication of implants for cartilage regeneration.

We used extrusion-based bioprinting to deposit ACPCs aggregates in PCL melt electrowritten scaffolds. The aim of the study was to show the suitability of this approach by investigating the viability and metabolic activity of the aggregates bioprinted on flat and tilted substrates.

2. Materials and methods

2.1 Cartilage component

Gelatin methacryloyl (gelMA) was synthesized as previously described [29]. Briefly, gelatin isolated from porcine skin and dissolved in phosphate-buffered-saine (PBS) to reach a concentration of 10% w/v at 60°C. Methacrylic anhydride (Sigma Aldrich) was added to reach the 80% degree of functionalisation. Freeze-dried gelMA was diluited with PBS to achieve the final gelMA concentration of 10% w/v and rotated at 37° C to ensure a homogeneous solution. The solution was added to the harvested ACPCs aggregates and 2,5% v/v Ruthenium (Sigma Aldrich) and 2,5% v/v Sodium Persulfate (SPS, Sigma Aldrich) were subsequently added to solution to initiate the cross-linking reaction. The constructs were crosslinked for 7 min under the flood light.

2.2 In vitro cell culture

Equine derived articular cartilage-resident progenitor cells (ACPCs) were obtained from the Efina equine donor. These donors have been donated to science by their owners and procedures were followed according to the guidelines of the Ethical and Animal Welfare body of Utrecht University. The cells were thawed from liquid nitrogen and expanded for 10 days. The expansion medium was composed of Dulbecco's modified eagle's medium GlutaMAX supplemented with 10% v/v fetal bovine serum (FBS),

1% v/v ascorbic acid (ASAP), 1% v/v Penicillin-Streptomycin (P/S, Gibco) and 0.5% v/v basic fibroblast growth factor (βFGF).

After the extrusion-based bioprinting process, the constructs were kept in culture in chondrogenic medium. It was composed of Dulbecco's modified eagle's medium GlutaMAX supplemented with 1% v/v ascorbic acid (ASAP), 1% v/v Penicillin-Streptomycin (P/S, Gibco), 1% v/v ITS Premix (Corning), 0.004% v/v Dexamethasone (Sigma) and 0.01% v/v TGFβ1 (Perprotech).

2.3 Chondrogenic aggregate fabrication

The stamps to pattern the agarose in which the cells were seeded were designed by using Catia CAD software. The design was inspired by Futrega et al. and the pyramidal design was reproduced in 2 sizes (medium and large) (Figure 2) to pattern 12 well plates (CELLSTAR®). The files were printed using the Perfactory 4 Mini ERM (EnvisionTEC) and the EnvisionTEC R5 resin.

Agarose plates were produced with and without the inclusion of melt electrowritten meshes according to the protocol (Supplementary data 1). Briefly, agarose (SeaKem® LE) was diluited with PBS to reach the final agarose concentration of 4% w/v. The solution was heated up using the microwave (SIEMENS) to ensure a homogeneous solution and get rid of air bubbles.

The medium-sized stamps consisted of 1209 microwells and were used to achieve a cell density of 1500 cells/microwell (group 1), while the large-sized stamps consisted of 769 microwells and were used for both the cell densities of 6000 cells/microwell (group 2) and 9000 cells/microwell (group 3).

According to the protocol, the cells were left in culture overnight to let them clump. At day 1 the aggregates were harvested and filtered with the EASYSTRAINER 40 μm (Greiner) to avoid the presence of single cells.

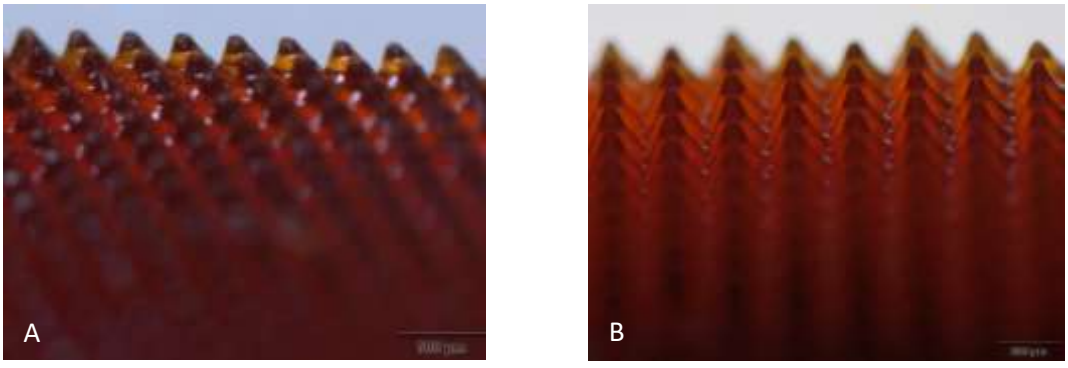

Figure 2: medium (A) and large (B) sized stamps.

2.4 Fibre reinforcing component

For all experiments PCL (PURASORB PC 12, Lot# 7500143428, 07/2023, Corbion Inc., Gorinchem, Netherlands) was used for melt electrowriting (MEW) (3D Discovery, RegenHU). PCL pellets were molten in a metallic cartridge at 80°C. A metal flat-tipped nozzle (30G, Unimed Switzerland) was heated and connected to a high voltage source.

A 30G nozzle, air pressure of 220 kPa, voltage of 6 kV, collector velocity of 12 mm/s, and a constant collection distance of 2 mm were applied to generate PCL fibre scaffolds.

Fibres were deposited onto uncoated glass slides with 300 layers to reach a height of approximately 1.8 mm. The melt electrowritten scaffolds had a "box-like" design with pores of 400 µm x 400 µm in programmed spacing.

2.5 Aggregate behaviour in 10% gelMA

To assess the behavior of the aggregates in the 10% gelMA matrix, discs with different densities of cells as aggregates were produced with and without the inclusion of melt electrowritten meshes according to the protocol (Supplementary data 2). Briefly, the ACPCs aggregates were harvested at day 1 and were included in 10% gelMA. For the groups III and VI (Table 3), melt electrowritten meshes were reshaped to a scaffold with a diameter of 6 mm by means of biopsy punch and included in the teflon moulds and 0.9 mL of solution consisting of 10% gelMA, aggregates, SPS and Ruthenoim was pipetted inside the moulds. The constructs were crosslinked under led light (20W LED, JOBMATE, China) for 7 minutes and subsequently keept in culture in chondrogenic differentiation medium (section 2.2) for 7 days.

Table 3: Experimental groups.

Groups	Cells per microwell	Density of cells as aggregates	Inclusion of MEW meshes
I	$7*10^3$ (L7000)	$10*10^6$/mL	No
II	$7*10^3$ (L7000)	$20*10^6$/mL	No
III	$7*10^3$ (L7000)	$10*10^6$/mL	Yes
IV	$8*10^3$ (L8000)	$10*10^6$/mL	No
V	$8*10^3$ (L8000)	$20*10^6$/mL	No
VI	$8*10^3$ (L8000)	$10*10^6$/mL	Yes

The metabolic activity of the aggregates embedded in the 10% gelMA at day 1 was assessed using the Alamar blue (AB) assay (Thermo Fisher Scientific) according to the manufacturer's protocol.

Briefly, alamarBlue reagente as added to the wells and it was incubated at 37 degrees C for 1-4 hours and the fluorescence was subsequently read. The results of the AB assays were read through the CLARIOstar Plus plate reader (BMG LABTECH).

2.6 Bioprinting aggregates in flat MEW meshes

To assess whether the extrusion-based bioprinting is a promising technique to accurately deposit aggregates inside the melt electrowritten "box-like" scaffolds, printability on a flat MEW meshes was investigated. Two cell densities ($1.0*10^7$ cells/mL and $2.0*10^7$ cells/mL, Table 4 and Table 5 respectively) were compared in order to individuate the proper density to fill the pores of the scaffold.

Table 4: Experimental groups deposited with a cell density of $1.0*10^7$ cells/mL.

Cell density: $1.0*10^7$ cells/mL	Stamp size	Cells/microwel
Group 1	Medium	1500
Group 2	Large	6000
Group 3	Large	9000

Table 5: Experimental groups deposited with a cell density of $2.0*10^7$ cells/mL.

Cell density: $2.0*10^7$ cells/mL	Stamp size	Cells/microwel
Group 1	Medium	1500
Group 2	Large	6000
Group 3	Large	9000

The ACPCs aggregates were harvested and divided into the 3 groups previously indicated into 50 mL tubes. Dry gelMA was dissolved in PBS to obtain the desired amount of 10% gelMA. The extrusion-based bioprinter (R-Gen200, Regenhu) was sterilized with 70% ethanol and UV light for 2 hours. The pneumatic pressure applied to extrude the aggregate-laden hydrogel was set in the range of 30-40 kPa. 10% gelMA without aggregates was printed as control group to check the functionality of the crosslinkers (SPS and Rithenium). Sterile gelMA was added to the 3 groups of aggregates to reach the desired cell density. The solutions were pipetted in 3 mL catridges (Nordson). Via SmoothFlow Tapered Dispense Tips (Nordson) with a 0.41 mm diameter the solution was dispensed on top of the box-structured MEW scaffolds. After printing, the constructs were crosslinked for 7 minutes under the flood light and cultured for 7 days in chondrogenic medium (Section 2.2).

Metabolic activity of the aggregates embedded in the 10% gelMA at day 1 and 7 was assessed using the Alamar blue (AB) assay (Thermo Fisher scientific) according to the manufacturer's protocol as explained in the precious section.

The viability of the aggregates in the "box-like" scaffolds was assessed using the LIVE/DEAD assay (Calcein, Ethidium homodimer, Thermo Fischer Scientific) according to the manufacturer's protocol. Briefly, 5 µL calcein and 20 µL ethidium were added to 10 mL of DPBS, the medium was removed from cells and 100-200 µL of solution was added to the cells. The incubation time was 30 min at 20-25 degrees C and the cells were subsequently washed with DPBS and imaged.

2.7 Bioprinting aggregates in tilted MEW meshes

To investigate more anatomically relevant shapes, the printability of aggregate-laden gelMA on tilted MEW scaffolds the printing experiment of the previous section was repeated under a 10 degrees angle and under a 30 degrees angle. The cell density used for both the printing experiments under a 10 and a 30 degrees angle was $2.0*10^7$ cells/mL and the experimental groups are shown in the Table 6 and Table 7 respectively. The only parameter that changed was the pneumatic pressure applied to extrude the aggregate-laden gelMA, set in the range of 15-25 kPa

Table 6: Experimental groups bioprinted under a 10 degrees angle.

Cell density: $2.0*10^7$ cells/mL	Stamp size	Cells/microwel
Group 1	Medium	1500
Group 2	Large	6000
Group 3	Large	9000

Table 7: Experimental groups bioprinted under a 30 degrees angle.

Cell density: $2.0*10^7$ cells/mL	Stamp size	Cells/microwel
Group 1	Medium	1500
Group 2	Large	6000
Group 3	Large	9000

As described in the previous section, AB assay and live/dead assay were performed to check if the aggregates are able to survive the extrusion-based bioprinting process and to assess how well they possibly survive after 1 and 7 days.

2.8 Imaging

Images of the stamps to pattern the agarose wells were obtained using the Transmitted Light microscope SZ61 (Olympus). The aggregates were imaged through the Inverted LED microscopes, DMi1 (Leica). The images were edited by using Fiji software (ImageJ).

The pictures of the LIVE/DEAD assay were taken by using THUNDER Imager Live Cell & 3D Assay (Leica).

2.9 Statistical analysis

The diameter of the aggregates was characterized by using Fiji software (ImageJ). All statistical analyses and graphs were generated using GraphPad Prism 8 software.

For the statistical analyses, the Mann-Whitney test was used to investigate the difference between the aggregates formed using 7000 and 8000 cells in terms of metabolic activity.

To test the difference between the aggregates formed using 1500, 6000 and 9000 cells, the Kruskal-Wallis test was performed to individuate a possible significant difference in terms of metabolic activity, viability and distance of the deposited aggregates. In such case, the Mann-Whitney test was performed to investigate the groups showing significant difference. A difference was determined to be significant when $p < 0.05$. Data is presented as mean ± standard deviation.

3. Results

3.1 Aggregate behaviour in 10% gelMA

The ACPCs aggregates were succesfully embedded in 10% gelMA both with and without the inclusion of melt electrowritten meshes. After 7 days the aggregates started adhering to the surrounding hydrogel (Figure 3C).

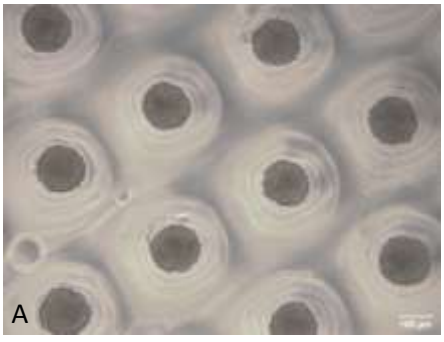

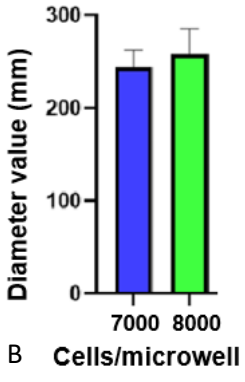

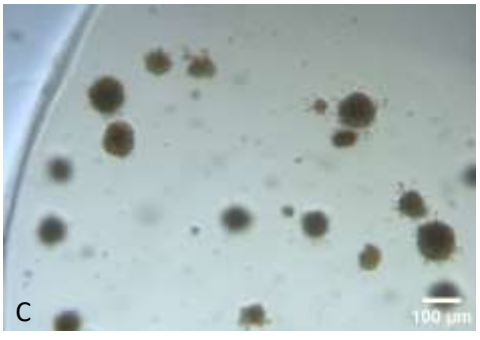

Figure 3: Aggregate formation and characterization, 5X magnification. Error bars represent standard deviations (B).

The metabolic activity of the aggregates formed by using 8000 cells/microwell, resulted to be significantly different between the constructs with a concentration of $1.0*10^7$ cells/mL with (6014.50 ± 822.46) and without MEW meshes (5257.00 ± 2083.74), with respect to the constructs with a concentration of $2.0*10^7$ cells/mL (8952.833 ± 1227.07).

No significant difference was found between the constructs embedding the aggregates formed by using 7000 cells/microwell with and without MEW meshes. Overal, no significant difference was found in terms of metabolic activity between the constructs including the MEW meshes and those not including the MEW meshes for both the sizes of aggregates (Figure 4). At day 1, the values of the metabolic activity is not significantly higher for the aggregates formed by using a cell density od 7000 cells/microwell.

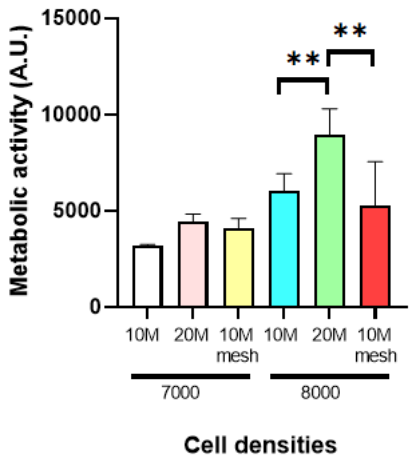

Figure 4: Metabolic activity of ACPCs aggregates after one day. Error bars represent standard deviations. ** = $p < .01$ (n=6).

3.2 Bioprinting aggregates in flat MEW meshes

ACPCs aggregates were succesfully bioprinted in flat MEW scaffolds by using two cell densities. The aggregate were characterized in terms of diameter (Figure 5).

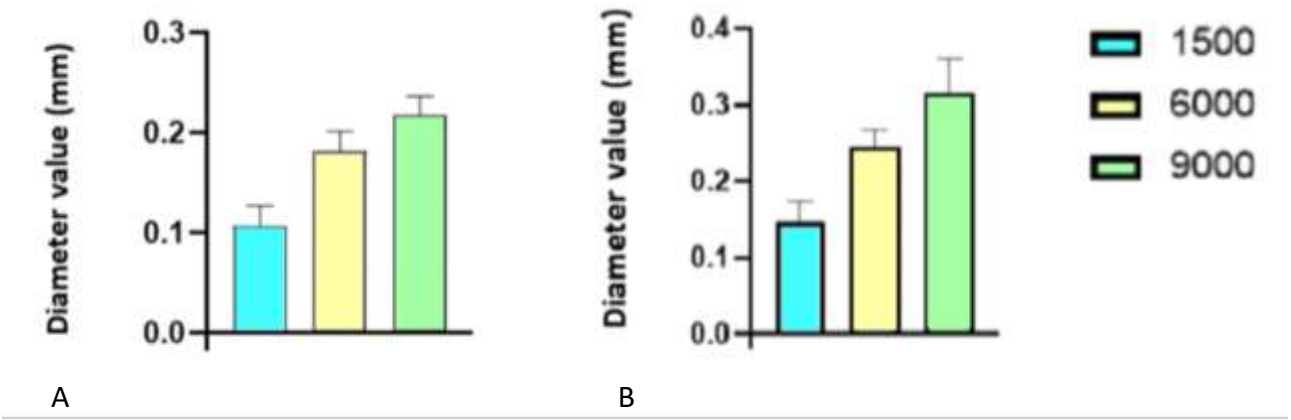

Figure 5: Diameter of the aggregates for the groups 1, 2 and 3 with a cell density of $1.0*10^7$ cells/mL (A) and $2.0*10^7$ cells/mL (B). Error bars represent standard deviations. (n = 63 for each group).

The use of various cell densities allowed to form aggregates with different diameters. In particular, the increase of the numer of cells per microwell allowed the formation of aggregates with larger diameters.

All the groups showed slight not significant decrease in terms of metabolic activity of the bioprinted aggregates over the course of 7 days for the cell dentisy of $1.0*10^7$ cells/mL, (5826.50 ± 150.50) at day 1 vs (4604.00 ± 16.0) at day 7, (5370.00 ± 44.00) at day 1 vs (4570.50 ± 6.50) at day 7, (5338.00 ± 23.00) at day 1 vs (4712.00 ± 0.00) at day 7, for the groups 1, 2 and 3 respectively (Figure 6A).

Upon quantification of the viability of the aggregates over the course of 7 days, no significant difference was detected between the groups for the cell density of $1.0*10^7$ cells/mL (Figure 6). The group 1 showed slight not significant decrease in the viabilty of the aggregates (78.39 ± 0.89) % at day 1 vs (70.95 ± 13.81) % at day 7. The groups 2 and 3 resulted in non significant increase terms of viability of the aggregates (67.44 ± 7.42) % at day 1 vs (76.25 ± 3.92) % at day 7 and (55.15 ± 5.86) % vs (62.79 ± 18.98) % at day 7, for the groups 2 and 3 respectively (Figure 6B).

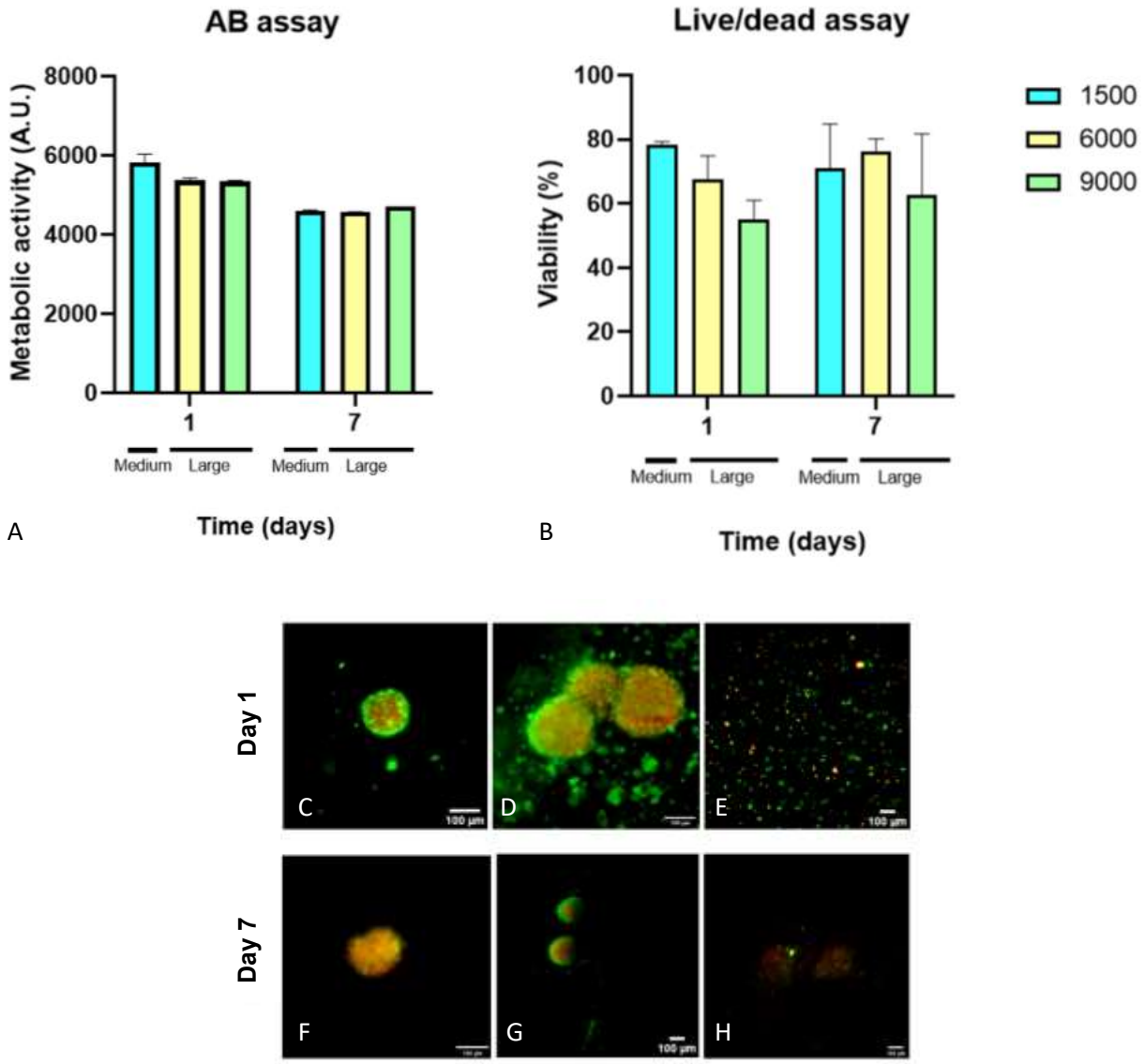

Figure 6: Viability and metabolic activity of ACPCs aggregates with a cell density of $1.0*10^7$ cells/mL over the course of 7 days. Error bars represent standard deviations (n = 3 for each group). Calcein (green) and ethidium (red) staining live/dead cells. Group 1 (C, F), group 2 (D, G), group 3 (E, H).

The groups 1 and 2 showed slight not significant decrease in terms of metabolic activity of the bioprinted aggregates over the course of 7 days for the cell dentisy of $2.0*10^7$ cells/mL, (2595.00 ± 18.00) at day 1 vs (2334.00 ± 13.00) at day 7, (2561.50 ± 32.50) at day 1 vs (2479.50 ± 15.50) at day 7, for the groups 1, 2 respectively. The metabolic activity of aggregates of group 3 showed slight not significant increase (2687.00 ± 21.00) at day 1 vs (2693.50 ± 73.50) at day 7.

Upon quantification of the viability of the aggregates over the course of 7 days, no significant difference was detected between the groups for the cell density of $2.0*10^7$ cells/mL (Figure 6). The groups 1 and 2 showed slight not significant decrease in the viabilty of the aggregates, (75.08 ± 1.16) % at day 1 vs (68.86 ± 4.62) % at day 7 and (77.07 ± 6.04) % at day 1 vs (72.61 ± 13.76) % at day 7 for the groups 1 and 2 respectively (Figure 7A).

The group 3 resulted in non significant increase terms of viability of the aggregates (49.65 ± 0.02) % at day 1 vs (59.24 ± 0.69) % at day 7. For both the experiments performed using flat MEW meshes the viability of the group 3 resulted to be lower than the groups 1 and 2 at both the time points (Figure 7B).

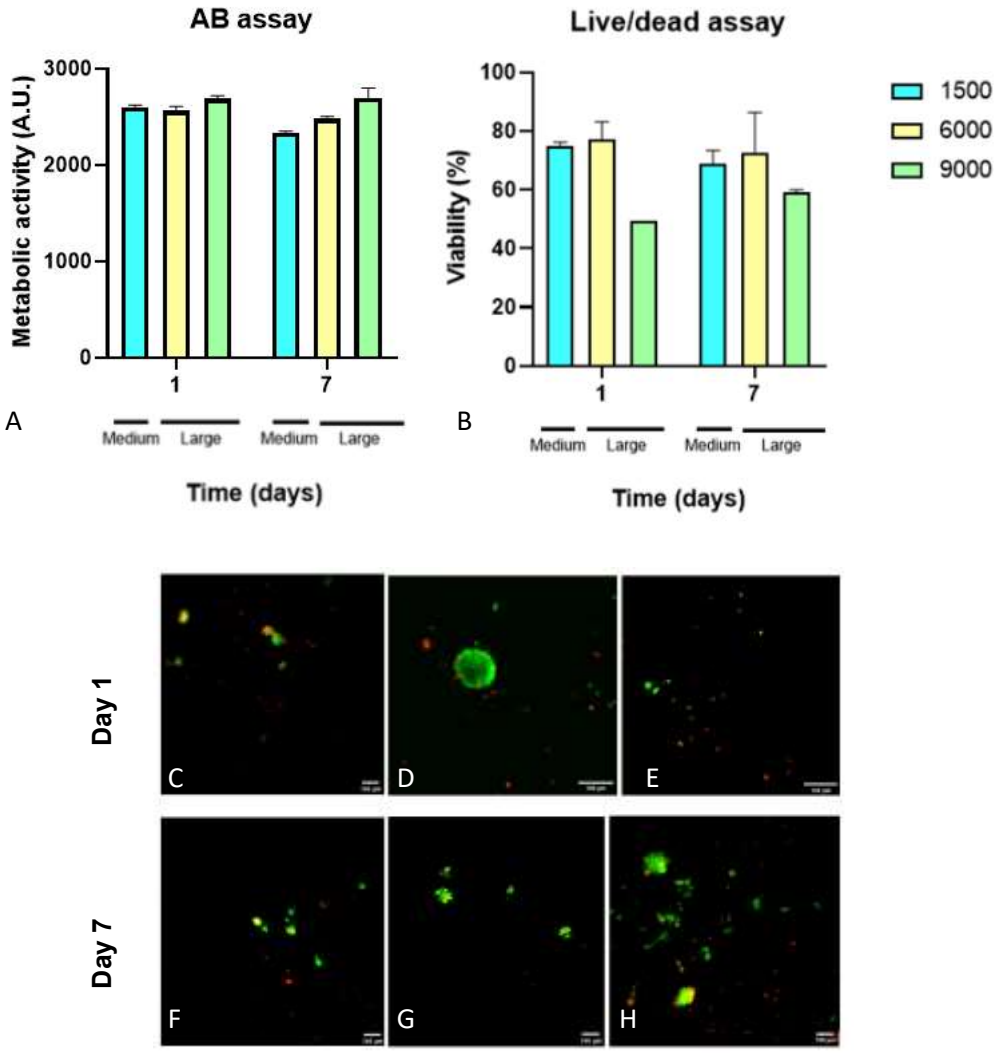

Figure 7: Viability (n=2) and metabolic activity (n=3) of ACPCs aggregates with a cell density of $2.0*10^7$ cells/mL over the course of 7 days. Error bars represent standard deviations (n = 3 for each group). Calcein (green) and ethidium (red) staining live/dead cells. Group 1 (C, F), group 2 (D, G), group 3 (E, H).

In order to evaluate the influence of the gravity on the deposition of the aggregates inside the melt electrowritten scaffolds with a box structure, the distance among the aggregates deposited during the bioprinting process was monitored over a period of 10 minutes. The distance was measured at time points of 5 minutes. The group 3 was investigated as the gravity has a greater effect on the deposition of the aggregates including a larger amount of cells. The distance between the aggregates at different time points dramatically decreased. Significant difference was found among all the groups (Figure 8).

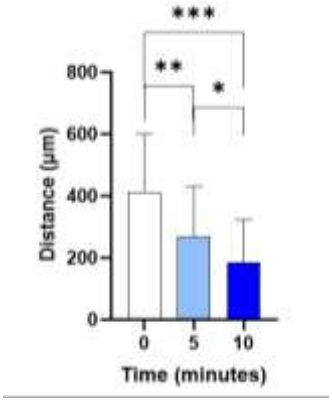

Figure 8: Distance among the deposited aggregates at different time points. Error bars represent standard deviations. * = p < .05** = p < .01. *** = p < .001 (n=25 for each group).

3.3 Bioprinting aggregates in tilted MEW meshes

ACPCs aggregates were succesfully bioprinted in flat MEW scaffolds under 10° and 30°. The aggregate were characterized in terms of diameter (Figure 9).

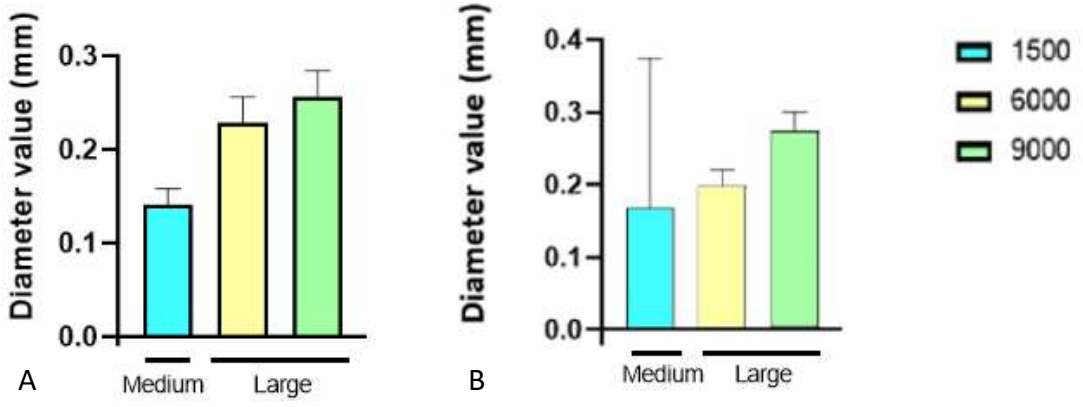

Figure 9: Aggregate diameter for the groups 1, 2 and 3 printed under 10° (A) and 30° (B). Error bars represent standard deviations, (n = 63 for each group).

The diameter of the aggregates showed the same trend as described in the previous section.

The metabolic activity of the aggregates bioprinted under 10° showed slight not significant decrease for the groups 1 (18902.50 ± 856.50) at day 1 vs (13821.50 ± 1119.50) at day 7. The metabolic activity showed little not significant increase (17132.00 ± 388.50) at day 1 vs (20125.50 ± 6100.50) at day 7 and (17087.00 ± 100.50) at day 1 vs (17758.50 ± 3708.50) at day 7 for the groups 2 and 3 respectively (Figure 10A).

Upon quantification of the viability of the aggregates over the course of 7 days, no significant difference was found over 7 days for the aggregates bioprinted under 10° (Figure 6). All the groups showed slight not significant decrease in the viabilty of the aggregates, (67.97 ± 0.28) % at day 1 vs (70.42 ± 0.78) % at day 7, (65.24 ± 4.14) % at day 1 vs (66.40 ± 3.59) % at day 7, (68.61 ± 6.24) % at day 1 vs (75.73 ± 0.99) % at day 7 for the groups 1, 2 and 3 respectively (Figure 10B).

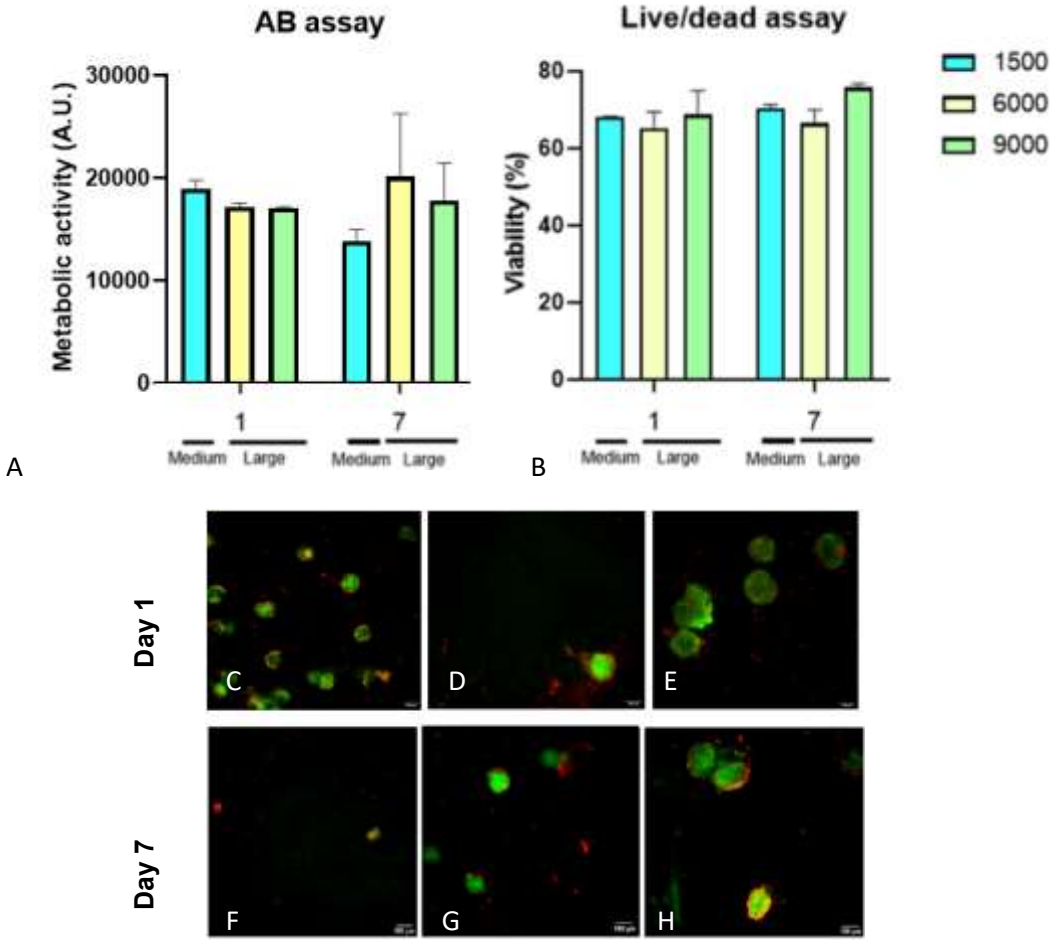

Figure 10: Viability (n=2) and metabolic activity (n=3) of ACPCs over the course of 7 days. Error bars represent standard deviations (n = 3 for each group). Calcein (green) and ethidium (red) staining live/dead cells. Group 1 (C, F), group 2 (D, G), group 3 (E, H).

All the groups of aggregates bioprinted under 30° showed slight not singificant decrease in terms of metabolic activity over the course of 7 days not significantly decreased for all the groups: (2856.50 ± 15.00) at day 1 vs (1989.00 ± 34.00) at day 7, (3754.00 ± 158.00) at day 1 vs (2602.00 ± 17.00) at day 7, (3630.00 ± 6.00) at day 1 vs (2966.50 ± 50.50) at day 7 for the groups 1, 2 and 3 respectively (Figure 11A).

The viability of the aggregates not significantly increased over 7 days for all the groups. The groups 1 and 2 showed slight significant increase in terms of viability, (75.81 ± 4.20) % at day 1 vs (79.72 ± 4.07) % at day 7, (65.84 ± 0.71) % at day 1 vs (68.45 ± 0.57) % at day 7, respectively. The group 3 showed slight not singificant decrease in terms of metabolic activity: (79.42 ± 0.60) % at day 1 vs (68.45 ± 0.57) % at day 7 (Figure 11B).

Overal, the viability of the aggregates of the group 3 bioprinted under 10° and 30° was higher than the viability of the same group bioprinted on top of flat MEW meshes.

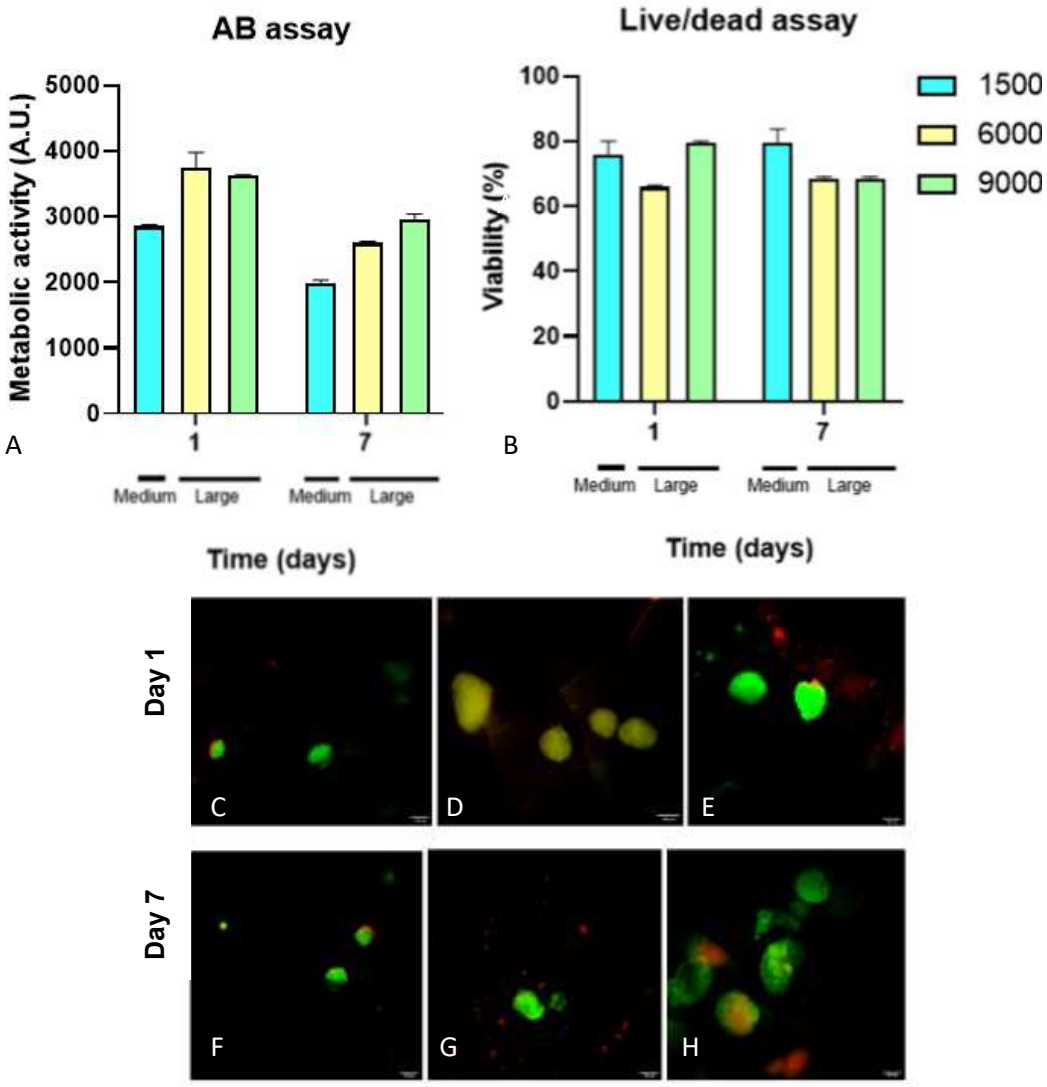

Figure 11: Viability (n=2) and metabolic activity (n=3) of ACPCs over the course of 7 days. Error bars represent standard deviations. Calcein (green) and ethidium (red) staining live/dead cells. Group 1 (C, F), group 2 (D, G), group 3 (E, H).

3.4 Bioprinting efficiency

The extrusion-based bioprinting process was evaluated in terms of percentage of volume occupied by the aggregates. The volume of the aggregates was calculated according to the obtained diameters, assuming to be spherical (Figure 13A).

The efficiency (η) of the bioprinting process was evaluated for a flat and for a tilted condition (Figure 13B). The calculations were made according to the scheme proposed in Figure 12. The total amount of filled pores was individuated manually (n_{filled}) and they were normalized to the total amount of

pores detected in the image. The efficiency was overally higher when printing on top of flat MEW meshes, than on top of tilted meshes.

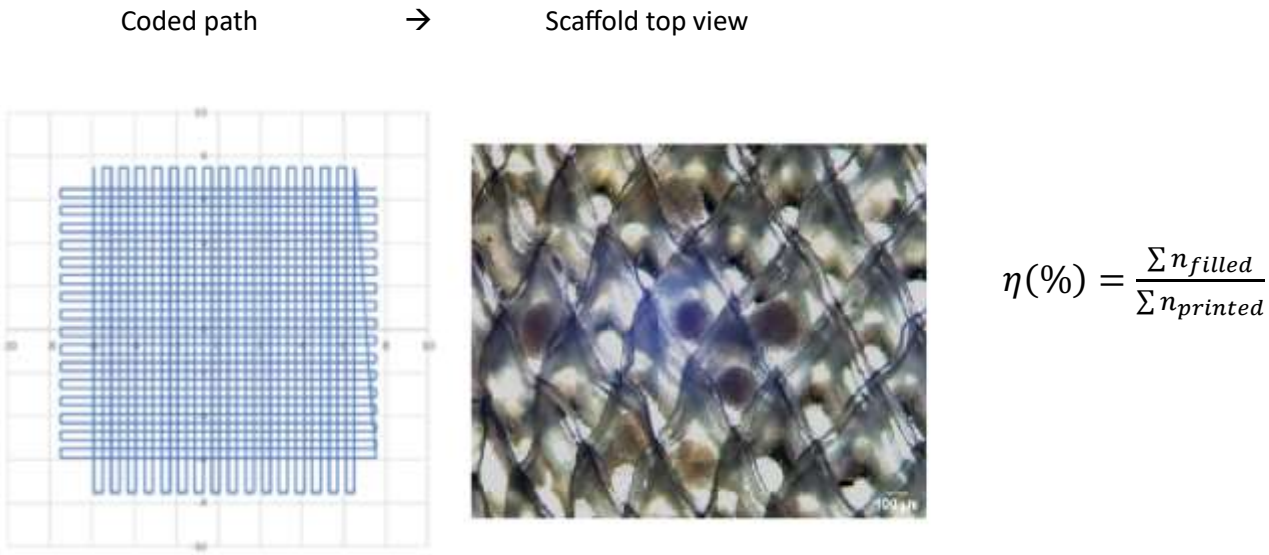

Figure 12: Method to quantify the efficiency of the extrusion-based bioprinting process.

The efficiency (η) of the extrusion-based bioprinting process was lower for all the groups when the extrusion-based bioprinting process was performed in tilted MEW meshes, with respect to the process performed in flat MEW meshes, (22.41 ± 23.78) % flat vs (9.11 ± 1.10) % tilted, (13.74 ± 1.78) % flat vs (12.5 ± 0.00) % tilted and (12.53 ± 7.94) % flat vs (12.22 ± 1.02) % tilted, for the groups 1, 2 and 3 respectively.

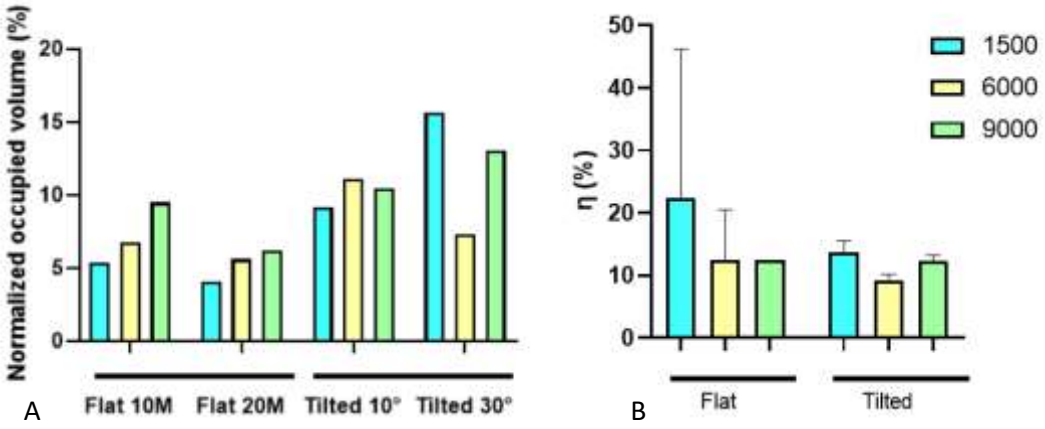

Figure 13: Quantification of the normalized occupied volume (A) and efficiency of the extrusion-based bioprinting process (B) (n = 3 for each group). Error bars represent standard deviations.

4. Discussion

In order to mimic patient joint morphology, this study focuses on placing aggregates into MEW meshes under different angles. The angles investigated ranged between 0° to 30° to reflect native joint morphology. Previous studies showed the suitability of MEW to collect fibres onto curved surfaces, and extrusion-based was proved to allow the deposition of cell-laden hydrogel on top of curved MEW meshes [30].

This study showed the successful and viable placement of aggregates in MEW meshes. MEW was previously combined with aggregates to allow for collagen guidance [31] with the purpose of achieving a cartilage-like structure. The average diameter of the aggregates achieved in this study is (0.207 ± 0.06) μm and literature shows similar sizes of aggregates made with Mesenchymal stem cells (MSCs) or chondrocytes [32].

The characterization of the aggregate behaviour in 10% gelMA showed that the presence of melt electrowritten meshes does not to influence the metabolic activity of the aggregates after 1 day. Further investigations are needed to assess the chondrogenic differentiation of the aggregates.

Similar trends were individuated in terms of metabolic activity after the deposition of the aggregates via extrusion-based bioprinting. For all the groups, the metabolic activity was mantained over the course of 7 days.

The aggregates did not show any significant variation over the course of 7 days in all the investigated groups after the deposition in flat and tilted MEW meshes. The LIVE/DEAD assay also allowed to visualize the spatial distribution of the cells in the scaffold. It was noticed that the aggregates of the group 3 split into single cells (Figure 6E, Figure 6H, Figure 7E, Figure 7H). This may indicate that the aggregates were subjected to high shear stress during the bioprinting process. Several studies reported shear stress to be the main cause of cell damage/death in the extrusion-based bioprinting process [33, 34]. As showed in Figure 6B and Figure 7B the viability of the aggregates is slightly lower for the group 3, remarking that the mechanical force might have affected the viabilty of the aggregates. The use of dispense tips with a larger diameter than the one used in this study may attenuate the effect of mechanical forces on the cell component. Another factor that might have contributed to the high shear stress is the applied pressure. To test this hypothesis, a slightly lower pressure was used to extrude the hydrogel on top of flat tilted meshes.

Furthermore, the aggregates resulted to be unevenly distributed in the scaffold. The hypothesis is that the gravity might have affected the distribution of the aggregates inside the nozzle before the deposition. To verify this hypothesis, the distance between the aggregates deposited in the stabilization lines was monitored over a period of 10 minutes. Significant differences were found between all the investigated groups (Figure 8), confirming that the gravity strongly influences the dispersion of the aggregates on top of the scaffold. The impossibility to mix the solution before extruding the bioink strongly influences the distribution of the aggregates. A valid option to improve this aspect is the use of a mixing chamber able to mix the bioink inside the nozzle before the extrusion, without affecting the viability of the cells [35].

When the experiment was repeated to deposit the aggregates in tilted melt electrowritten "box-like" scaffolds, the viability and metabolic activity of ACPCs aggregates remained stable over the course of 7 days. The gravity affected the distribution of the aggregates inside the nozzle as well as their deposition after the extrusion of the bioink. In addition, the viability of the group 3 notably increased with respect to the previous experiments. This confirmed the previous hypothesis that the pneumatic pressure applied to the aggregate-laden hydrogel can affect the viability of the aggregates during the bioprinting process.

The hydrophilicity of the PCL scaffold, delays the entry of the bioink inside the meshes. As a result, the distribution of the aggregates in the scaffold, already subjected to the effect of the gravity inside the nozzle, was further boosted after the extrusion-based bioprinting process, leading to an higher concentration of aggregates in the boxes of the scaffold at the lowest z-points. The use of sodium hydroxide solution was shown to improve the hydrophilicity of PCL melt electrowritten scaffolds [36] and it could further improve the even distribution of the aggregates inside the "box-like" scaffold. Thus, tilted substrates still represent a major limitation for extrusion-based bioprinting on top of melt electrowritten scaffolds. Future studies may investigate the deposition of aggregates by using a larger range of angles, eventually moving to a curved substrate.

A relevant aspect that can be further improved is the efficiency of the extrusion-based bioprinting process. Performing the extrusion-based bioprinting process on top of tilted surface highly affects the efficiency due to the uneven distribution of the aggregates. On the other hand, already after 1 day the aggregates started merging (Figure 6D), hypothetically secreting ECM. The hypothesis is that the aggregates will further merge and secrete ECM components over time. Monitoring the aggregates over a longer period can prove that the aggregates can secrete collagen all over the scaffold, guided by the meshes of the scaffold. If this hypothesis will be proved by future works, the cell density of

$2.0*10^7$, would be enough for the purpose of achieving collagen structures resembling those of the native tissue.

In order to confirm this hypothesis, further studies may perform histological analysis to investigate the secretion of the proteoglycans and collagen type II. Immunohistochemical analysis may be performed to assess whether the collagen resembles the structure of the native tissue.

5. Conclusions

In this study melt electrowriting and extrusion-based biopriting were converged to fabricate scaffolds for articular cartilage regeneration *in vitro*. Chondrogenic aggregates were succesfully formed, included in a biocompatible hydrogel and deposited inside melt electrowritten "box-like" scaffolds. The quantification of the metabolic activity and viability of the aggregates over 7 days showed the suitability of extrusion-based bioprinting for the deposition of aggregates on top of flat and tilted MEW meshes.

This study paves the way for bioprinting on top of anatomically relevant surfaces, including curved substrates, to more closely resemble patient-specific defects. The outcomes of the study highlight the advantage of converging biofabrication techniques to ensure a "cartilage-like" environment to the cells. Future studies could further investigate the effect of the guidance of the MEW meshes and the chondrogenic differentiation of the aggregates to ensure the formation of a cartilage-like environment.

References

[1] Yumei Li et al. Recent Advances in Understanding the Role of Cartilage Lubrication in Osteoarthritis. Molecules 2021, 26(20), 6122; https://doi.org/10.3390/molecules26206122

[2] Alice J. Sophia Fox, Asheesh Bedi, Scott A. Rodeo. The Basic Science of Articular Cartilage. Sports Health. 2009 Nov; 1(6): 461–468.doi: 10.1177/1941738109350438

[3] JA Buckwalter, VC Mow, A Ratcliffe. Restoration of Injured or Degenerated Articular Cartilage. J Am Acad Orthop Surg.192-201. doi: 10.5435/00124635-199407000-00002

[4] R. Garrett Steinmetz et al. Global Variation in Studies of Articular Cartilage Procedures of the Knee: A Systematic Review. Cartilage. 2022 Apr; doi: 10.1177/19476035221098169

[5] A. Ghouri et al. The relationship between meniscal pathologies, cartilage loss, joint replacement and pain in knee osteoarthritis: a systematic review. Osteoarthritis Cartilage. 2022 Oct;30(10):1287-1327. doi: 10.1016/j.joca.2022.08.002

[6] S. Heir et al. Focal cartilage defects in the knee impair quality of life as much as severe osteoarthritis: a comparison of knee injury and osteoarthritis outcome score in 4 patient categories scheduled for knee surgery. Am J Sports Med. 2010 Feb;38(2):231-7. doi: 10.1177/0363546509352157

[7] Scotti et al. A tissue engineered osteochondral plug: an in vitro morphological evaluation. Knee Surg Sports Traumatol Arthrosc. 2007 Nov;15(11):1363-9. doi: 10.1007/s00167-007-0359-z

[8] Shuyu Liu et al. Cartilage tissue engineering: From proinflammatory and anti-inflammatory cytokines to osteoarthritis treatments. Mol Med Rep. 2022 Mar; 25(3): 99.Published online 2022 Jan 24. doi: 10.3892/mmr.2022.12615

[9] E. Carlos Rodrìguez-Merchán. Articular Cartilage Defects of the Knee: Diagnosis and Treatment. Springer Verlag; 2012th edition (20 October 2012)

[10] Marrit Hardenberg et al. The economic burden of knee and hip osteoarthritis: absenteeism and costs in the Dutch workforce. BMC Musculoskelet Disord. 2022 Apr 18;23(1):364. doi: 10.1186/s12891-022-05306-9.

[11] Mantas Malinauskas et al. Cartilage regeneration using improved surface electrospun bilayer polycaprolactone scaffolds loaded with transforming growth factor-beta 3 and rabbit muscle-derived stem cells. Front. Bioeng. Biotechnol., 23 August 2022 Sec. Biomaterials Volume 10 – 2022, https://doi.org/10.3389/fbioe.2022.971294

[12] Jason Koh et al. Small Chondral Defects Affect Tibiofemoral Contact Area and Stress: Should a Lower Threshold Be Used for Intervention? Orthop J Sports Med. 2022 Nov; 10(11): 23259671221129308. Published online 2022 Nov 17. doi: 10.1177/23259671221129308

[13] M P J van den Borne et al. International Cartilage Repair Society (ICRS) and Oswestry macroscopic cartilage evaluation scores validated for use in Autologous Chondrocyte Implantation (ACI) and microfracture. Osteoarthritis Cartilage. 2007 Dec;15(12):1397-402. doi: 10.1016/j.joca.2007.05.005. Epub 2007 Jul 2

[14] Jürgen Groll et al. Biofabrication: reappraising the definition of an evolving field. 2016 Jan 8;8(1):013001. doi: 10.1088/1758-5090/8/1/013001

[15] B. Zylinska.Treatment of Articular Cartilage Defects: Focus on Tissue Engineering. In Vivo. 2018 Nov-Dec; 32(6): 1289–1300. Published online 2018 Nov 3. doi: 10.21873/invivo.11379

[16] Peter A Levett et al. Chondrocyte redifferentiation and construct mechanical property development in single-component photocrosslinkable hydrogels. J Biomed Mater Res A. 2014 Aug;102(8):2544-53. doi: 10.1002/jbm.a.34924. Epub 2013 Sep 2.

[17] Madhavi Latha Chinta et al. Assessment of properties, applications and limitations of scaffolds based on cellulose and its derivatives for cartilage tissue engineering: A review. Int J Biol Macromol. 2021 Apr 1;175:495-515. doi: 10.1016/j.ijbiomac.2021.01.196. Epub 2021 Feb 2

[18] Sebastian Loewne et al. Recent advances in melt electro writing for tissue engineering for 3D printing of microporous scaffolds for tissue engineering. Front Bioeng Biotechnol. 2022; 10: 896719. Published online 2022 Aug 17. doi: 10.3389/fbioe.2022.896719

[19] Visser J, Melchels FPW, Jeon JE, et al. Reinforcement of hydrogels using three-dimensionally printed microfibres. Nat Commun. 2015;6:1-10. doi:10.1038/ncomms7933

[20] Bas O, De-Juan-Pardo EM, Meinert C, et al. Biofabricated soft network composites for cartilage tissue engineering. Biofabrication. 2017;9(2):25014. doi:10.1088/1758-5090/aa6b15

[21] Mylène de Ruijter et al. Out-of-Plane 3D-Printed Microfibers Improve the Shear Properties of Hydrogel Composites. Small. 2018 Feb;14(8):10.1002/smll.201702773. doi: 10.1002/smll.201702773. Epub 2017 Dec 14.

[22] Kai D, Prabhakaran MP, Stahl B, Eblenkamp M, Wintermantel E, Ramakrishna S. Mechanical properties and in vitro behavior of nanofiber-hydrogel composites for tissue engineering applications. Nanotechnology. 2012;23(9):95705. doi:10.1088/0957-4484/23/9/095705

[23] Katja Hölzl et al. Gelatin methacryloyl as environment for chondrocytes and cell delivery to superficial cartilage defects. J Tissue Eng Regen Med. 2022 Feb;16(2):207-222. doi: 10.1002/term.3273. Epub 2021 Dec 15.

[24] Santos Martinez-Diaz et al. In vivo evaluation of 3-dimensional polycaprolactone scaffolds for cartilage repair in rabbits. Am J Sports Med. 2010 Mar;38(3):509-19. doi: 10.1177/0363546509352448. Epub 2010 Jan 21.

[25] Craig A Simmons et al. Dual growth factor delivery and controlled scaffold degradation enhance in vivo bone formation by transplanted bone marrow stromal cells. Bone. 2004 Aug;35(2):562-9. doi: 10.1016/j.bone.2004.02.027.

[26] Margot Rikkers et al. The clinical potential of articular cartilage-derived progenitor cells: a systematic review. Nature. Published: 10 January 2022. DOI: https://doi.org/10.1038/s41536-021-00203-6

[27] Levato et al. The bio in the ink: cartilage regeneration with bioprintable hydrogels and articular cartilage-derived progenitor cells. Acta Biomater. 2017 Oct 1;61:41-53. doi: 10.1016/j.actbio.2017.08.005. Epub 2017 Aug 4.

[28] Ross Burdis et al. Spatial patterning of phenotypically distinct microtissues to engineer osteochondral grafts for biological joint resurfacing. Biomaterials. 2022 Oct;289:121750. doi: 10.1016/j.biomaterials.2022.121750. Epub 2022 Aug 28.

[29] Van Den Bulcke AI et al. Structural and Rheological Properties of Methacrylamide Modified Gelatin Hydrogels. Biomacromolecules. 2000;1(1):31-38. doi:10.1021/bm990017d

[30] Peiffer et al. Melt electrowriting onto anatomically relevant biodegradable substrates: Resurfacing a diarthrodial joint. Volume 195, October 2020, 109025. Materials & Design

[31] Andrew C Daly 1, Daniel J Kelly. Biofabrication of spatially organised tissues by directing the growth of cellular spheroids within 3D printed polymeric microchambers. Biomaterials. 2019 Mar; 197:194-206. doi: 10.1016/j.biomaterials.2018.12.028. Epub 2019 Jan 8.

[32] Guanhuier Wang. Chondrocyte Spheroids Laden in GelMA/HAMA Hybrid Hydrogel for Tissue-Engineered Cartilage with Enhanced Proliferation, Better Phenotype Maintenance, and Natural Morphological Structure. Gels. 2021 Dec; 7(4): 247. Published online 2021 Dec 2. doi: 10.3390/gels7040247

[33] Selwa Boularaoui. An overview of extrusion-based bioprinting with a focus on induced shear stress and its effect on cell viability. Bioprinting. Volume 20, December 2020, e00093
[34] Monize Caiado Decarli, Bioprinting of Stem Cell Spheroids Followed by Post-Printing Chondrogenic Differentiation for Cartilage Tissue Engineering. Adv Healthc Mater. 2023 Jul;12(19): e2203021. doi: 10.1002/adhm.202203021. Epub 2023 May 3.
[35] Will Hoggatt. Development of a fluidic mixing nozzle for 3D bioprinting. Biology, Engineering, Materials Science. Published 2016. Corpus ID: 51780163
[36] Zhu-Xing Zhou et al. Facile Strategy on Hydrophilic Modification of Poly(ε-caprolactone) Scaffolds for Assisting Tissue-Engineered Meniscus Constructs In Vitro. Front Pharmacol. 2020; 11: 471.Published online 2020 May 1. doi: 10.3389/fphar.2020.00471
[37] Juliane C Kade, Paul D Dalton. Polymers for Melt Electrowriting. Adv Healthc Mater. 2021 Jan;10(1):e2001232. doi: 10.1002/adhm.202001232. Epub 2020 Sep 17.
[38] Kamila Białkowska et al. Spheroids as a Type of Three-Dimensional Cell Cultures—Examples of Methods of Preparation and the Most Important Application. Int J Mol Sci. 2020 Sep; 21(17): 6225. Published online 2020 Aug 28. doi: 10.3390/ijms21176225
[39] Mingyue Sun et al. Synthesis and Properties of Gelatin Methacryloyl (GelMA) Hydrogels and Their Recent Applications in Load-Bearing Tissue. Polymers (Basel). 2018 Nov; 10(11): 1290. Published online 2018 Nov 21. doi: 10.3390/polym10111290

Acknowledgements

I would like to sincerely thank my examiner, Prof. Dr. Jos Malda for giving me the opportunity to work in his lab with the amazing “Malta Team”. Thanks to my supervisor Prof. Dr. Mylene de Ruijter for letting me manage this study, for teaching me how to become independent despite starting with no lab experience and for teaching me to ask for help when I need it. Thanks to Anneloes Mensinga for assisting me with cell culture, for showing me your valuable tips and for being my moral support. I will take the time spent together to heart. Thanks to Lennard Spauwen for guiding me through the melt electrowriting printing process and for providing your old MEW meshes for my preliminary experiments, you have been my last-minute life saver.

Thanks to Charlie, you have been literally with me from the first to the last day in the lab, my borrel-mate and my greatest fan. I hope we will share many other experiences together, starting from our trip to Portugal. To all my lab-mates, thanks for making this journey one of the most enjoyable I have ever experienced.

Thanks to my family and my Italian friends for celebrating my achievements and rooting for me from far away, I always bring all of you in my heart.